Journal of Materials Chemistry A

Accepted Manuscript

ROYAL SOCIETY OF CHEMISTRY

www.rsc.org/materialsA

Journal Name

COMMUNICATION

Ambient Pressure Dried Graphene Aerogels with Superelasticity and Multifunctionality

Received 00th January 20xx,
Accepted 00th January 20xx

DOI: 10.1039/x0xx00000x

www.rsc.org/

Hongsheng Yang, Tongping Zhang, Min Jiang, Yongxin Duan, and Jianming Zhang*

We report ambient pressure dried graphene aerogel (ADGA) with superelasticity (rapidly recoverable from >90% compression) and multifunctionality could be obtained with the ordinary instruments by recasting the partially reduced graphene oxide hydrogel (PRGH) with ice-template method. This study would be a key progress for realizing the cost-effective and large-scale commercial production of high-performance graphene aerogels.

Three-dimensional (3D) macroscopic materials assembled by the atom-thick two-dimensional (2D) graphene sheets with excellent mechanical, electrical and thermal properties[1-3] as well as the ease of scalable synthesis from inexpensive graphite[4, 5] have an exceptional potential in many practical applications[6-16]. Especially, ultralight graphene aerogels with high compressive and electrical properties hold great promise for energy dissipation, vibration damping, conductive sensor and recyclable absorbent for oil.[17-23] The excellent elasticity of these aerogels may attribute to the elastic nature of graphene sheet[24, 25] and integrated graphene walls consisting ordered 3D structure such as honeycomb-like[17-19] or spherical pores[20-22]. Currently, Sol-gel drying method[14-20] is considered as a relatively facile and scalable strategy to produce graphene aerogels. Of particular note, for obtaining the graphene aerogel with well-defined shape, it is necessary to replace the liquid inside gels by air using a special drying technique, such as freeze drying[17-22] or supercritical drying[14-15], which could leave the dry sample with minimal distortion of the gelled volume and structure. However, it is well known that the freeze drying and subcritical point drying techniques required special devices are too laborious and high cost.[11, 26-31] In contrast, ambient pressure drying (APD) technique is extremely convenient and energy-saving, without the utilization of special instruments supplied by high pressure, ultra-low temperature or vacuum environment. Therefore, ambient drying technique is strongly desired for large-scale and low-cost industrial production of graphene aerogel. Nevertheless, the capillary action caused by the evaporation of water cannot be avoided during the drying procedure under the ambient pressure. It usually results in the collapse of pore structure and is unfavourable for the preparation of the ultralight and elastic macroscopic materials.[11] Thus, it still remains a big challenge to fabricate graphene aerogels with ultralight and compressive properties by Sol-gel method based on the ambient pressure drying technique.

Here, we demonstrated for the first time that ambient pressure dried graphene aerogel (ADGA) with exceptional elasticity (rapidly recoverable from＞90% compression) could be successfully obtained with the ordinary instruments by recasting the partially reduced graphene oxide (GO) hydrogel (PRGH) with ice-template method. The resultant materials also exhibit the excellent cycling electrical conductivity and recyclable absorption capacity for oil.

The synthesis of ADGA was illustrated in Fig. 1a. Firstly, the PRGH was prepared by heating GO aqueous dispersion at 95 °C for certain time with the addition of L-Ascorbic acid (L-AA) as a mild reducing agent[17]. Then, the PRGH was completely frozen at -18 °C in an ordinary refrigerator followed by thawing at room temperature. After further reduction with prolonged time, the reduced graphene hydrogel (RGH) was dried in oven at ambient condition for 24 hours to get the ADGA. In the process of sample preparation, it is found that suitable reduction time for obtaining PRGH prior to freeze-thaw process is a key step to realize the ambient pressure drying of RGH without the shrink in volume. As shown in Fig. 1b-1d, it could be clearly seen that one hour is the optimal reaction time, in which the shape and volume of as prepared ADGA kept almost the same with original RGH. In contrast, more or less reduction time for preparing PRGH will lead to the obvious collapse or shrink of ADGA. By carefully controlling the reduction time, the ADGA with an ultralow density (ρ) ranging from 2.5 to 8.3 mg cm^{-3} (Fig. 1e), which belongs to the density

Key Laboratory of Rubber-Plastics, Ministry of Education/Shandong Provincial Key Laboratory of Rubber-Plastics, Qingdao University of Science & Technology, Qingdao City 266042, People's Republic of China
E-mail: zjm@qust.edu.cn
† Footnotes relating to the title and/or authors should appear here.
Electronic Supplementary Information (ESI) available: [details of any supplementary information available should be included here]. See DOI: 10.1039/x0xx00000x

range of graphene aerogel (<10 mg cm^{-3}),[37-39] could be prepared with GO concentration from 1 mg mL^{-1} to 5 mg mL^{-1} (Fig. S1, Electronic Supplementary Information). The inserted digital photo describing a sample stand on a dog's tail-like flower in Fig. 1e also showed the ultralight feature of thus prepared ADGA. It is worth mentioning that, dependent on the shape of reactor utilized, the proposed craft could not only successfully fabricate the cylindrical sample but also other arbitrary shapes such as rectangle, cone, frustum cone and sphere as displayed in Fig. 1f. It suggests that our method provides a chance to prepare shape-controlled ADGA as desired.

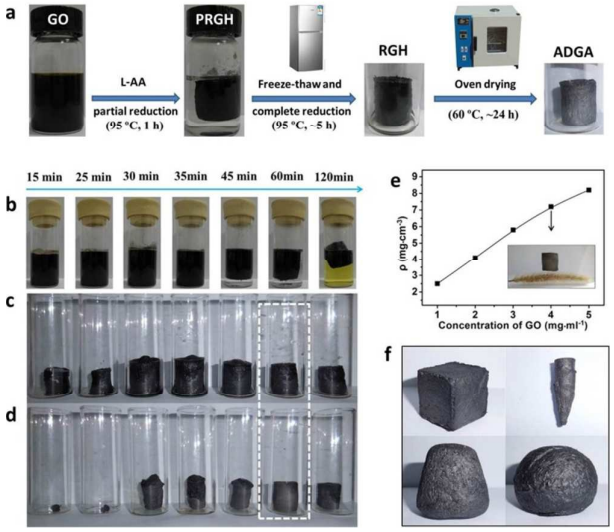

Fig. 1 (a) Illustration of the fabrication process of the ADGA. Digital images of different stages of time-dependent formation process: (b) PRGH with different reduction time; (c) RGH after freeze-thaw process from different PRGH; (d) different dried RGH after ambient pressure drying. (e) The density of ADGAs as a function of the concentration of GO; the insert picture showed the ADGA on a dog's tail-like flower. (f) Digital images of different shape ADGAs depend on different shape vessels.

In a recent work, Qiu et al.[17] reported that ultralight graphene monoliths with biomimetic cork-like hierarchical structure could be readily fabricated by freeze casting method via precisely controlling the reduction time of GO dispersion. However, the APD technique used to prepare graphene aerogels couldn't be realized in their work. Compared with Qiu's work, an important modification for us to realize the ambient drying lies in that we used the refrigerator (-18 °C) to freeze the partial reduced GO (pr-GO) gel at slower cooling rate rather than the dry ice (-78.5 °C) at very fast cooling rate. Previous studies[17, 33-35] have demonstrated that applying the freeze technique on aqueous suspension of nanoparticles offers a versatile approach to produce three dimensional porous structures, which are templated by the formation of ice crystal. Moreover, the higher cooling rates of freeze will result in smaller pore diameters as reported by Wicklein et al.[36] In other word, slower cooling rates of freeze in our crafts will lead to larger pore diameters.

As mentioned in introduction section, the aerogels obtained via APD usually showed a severely shrinkage or collapse of the wet gel in volume after drying due to the capillary pressure (P). The capillary pressure is related to the contact angle (θ), surface tension of the pore liquid (γ) and pore radius (r), according to the following Equation (Laplace formula[30, 31]).

$$P = (-2\gamma \cos(\theta)) / r$$

From this equation, it is clearly revealed that P will be inversely proportional to the pore radius (r) if contact angle (θ) and surface tension (γ) keep constant. Therefore, enlarging the pore radius of graphene gels will be a very effective path to minimize the capillary force, which is favorable for realizing the ambient drying.

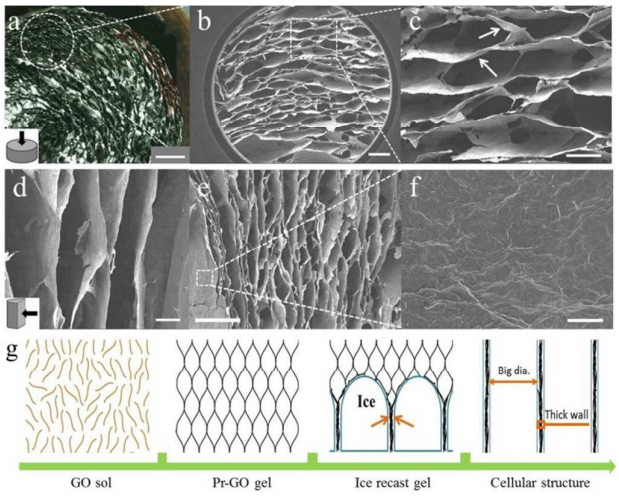

Fig. 2 Typical top-view (a-c) and side-view (d-f): (a) A stereoscopic microscope picture of cross section of ADGA. (b, c) SEM images of cross section of ADGA. (d, e) SEM images of vertical section of ADGA. (f) The enlarged SEM image of ADGA surface. Scale bars: (a) 2 mm, (b) 500 μm, (c, d) 200 μm, (e) 1 mm and (f) 10 μm. (g) Schematics showed the formation mechanism of the cellular structure of ADGA include the gelation process of GO and freeze recasting process of pr-GO gel.

Fig. 2a presents a typical stereoscopic microscope picture of superelastic ADGA cross section (top-view) with a density of 8.1 mg cm^{-3}. It shows that the inner graphene walls look like loops with different sizes surrounding the center. The scanning electron microscope (SEM) images with various magnification from different view angle (top-view, Fig. 2b-2c; side-view, Fig. 2d-2f) reveal that our ADGAs also exhibit the homeycomb-like and oriented cellular structure, which is similar to the cork-like structure reported by Qiu et al[17]. However, our ADGA samples presents obviously larger cell dimension in the order of hundreds of micrometers (ca.100~500 μm) than those of Qiu et al. (in the order of tens of micrometers). This observation confirmed the speculation mentioned above, that is, lower cooling rate will result in the formation of larger pore dimension in PRGH. Except the larger cell dimension, high-

resolution TEM analysis (Fig. S2, Electronic Supplementary Information) shows that the thickness of the wall for our ADGA (ca.200 nm) is also 10 times thicker than that of Qiu et al's sample. Moreover, high-resolution TEM also reveals that graphene sheets in the cell wall of our ADGA are closely packed and well oriented in parallel manner similar to the ultrastrong graphene paper prepared under the directional flow[40,41] These morphology observations suggest that graphene sheets assembled into strong oriented cells and continuous network could resist the smaller capillary stress caused by the bigger graphene pores so that the utralight graphene aerogels can be successfully produced by APD method. This is like the strong upright walls of a building support the monolith to avoid the collapse.

Fig. 2g illustrates the formation process of such cellular structure of ADGA. It should be pointed out that, different from the work of Qiu[17], more reduction time was used in our case so that the pr-GO sheets are gradually attracted via enhanced π–π interaction to form the weakly cross-linked hydrogel rather than kept them in suspension state. As shown in Table S1 (Electronic Supplementary Information), the optimal C/O value of PRGH around 3.01 (reduction time, 60 min) is bigger than the critical point of C/O value (~1.93) in that work. In the subsequently freeze-recast step, the growth of ice crystals then can break through the as formed weakly cross-linked graphene network and reject the graphene sheets into the neighboring ice crystals to form a continuous network with bigger pore dimensions. As evidenced in Fig. S1 (Electronic Supplementary Information), the π–π interaction between pr-GO sheets must be controlled to a certain extent, and too weak or too strong interactions are not suitable for the oriented growth of ice crystals at lower cooling rate to obtain the cork-like structure with bigger cell dimension and thicker cell wall, which is suitable for the ambient drying process.

The transformation from GO to the final graphene aerogel was examined by elemental analysis (Table S1, Electronic Supplementary Information), X-ray diffraction (XRD) (Fig. S3a, Electronic Supplementary Information), X-ray photoelectron spectroscopy (XPS) (Fig. S3b, Electronic Supplementary Information) and Raman spectroscopy (Fig. S3c, Electronic Supplementary Information). After fully reduced by the L-AA at 95 °C with 6 h, elements analysis data shows that the C/O value of ADGA increases up to 9.08 (Table S1, Electronic Supplementary Information), indicating most of functional groups are eliminated.[17] The typical diffraction peak for GO appears at around 10.43°, corresponding to the interlayer space (d) of 0.847 nm. Of particular interest is that new broadened diffraction peaks at 23.90° (inner wall) and 25.55° (outer wall), corresponding to the interlayer space of 0.372 nm and 0.348 nm, were found respectively in the inner and side surface layers of aerogel. These results revealed that not only π–π stacking between the graphene sheets but also different graphite-like structures in the graphene aerogel were formed and the surface graphene layers arrangement was more similar to the graphite (d =0.336 nm).[16, 43] The XPS tests further confirmed the disappearance of oxygen-containing groups after reduction.[42] In the Raman spectra, GO shows an I_D /I_G ratio of 0.93 while the average corresponding value for aerogel increases to ~1.22 after reduction. This indicates the π–π conjugated structure of graphene is partially restored in the as prepared aerogel.[42]

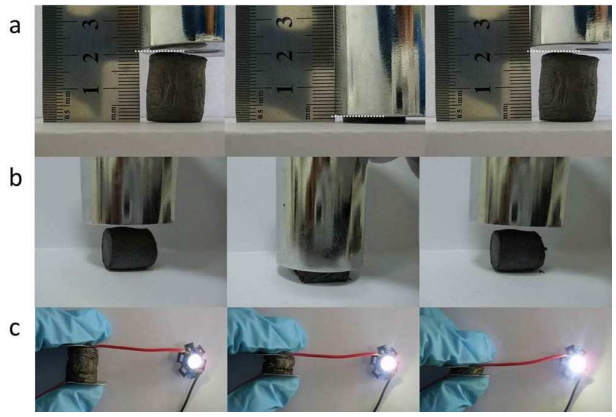

Fig. 3 Axial (a) and radial (b) compressive tests of the superelastic ADGA. (c) Snapshots of the decreasing electrical resistance of the ADGA under compression, where the higher compressive strain the stronger the brightness of the lamp is in the circuit.

The compressibility of ADGA is displayed in Fig. 3a, 3b. Considering the anisotropy microstructure of ADGA revealed in Fig. 2b, 2d, the compressive tests were respectively conducted along the axial direction and radial direction of the cylindrical sample. Along these two distinct directions, the ADGA can be both squeezed into a pellet under pressure but completely recover once the external pressure is removed. For the axial compressive test (Fig. 3a and Movie 1), the height of the graphene aerogel before compressing was greater than 20 mm, but only less than 2 mm under the weight stress. It reveals that our ADGA has the superelastic property and could be rapidly recoverable even when the compressive strain is above 90%. To the best of our knowledge, this result could be compared to the best performance reported so far. The results of cyclic compression testing with maximum strain up to 93% for ADGA are shown in Fig. 4a, which is consistent with the observation in Fig. 3a. More specifically, the ADGA was compressed and completely recovered for 3 cycles and the maximum compressive stress at 93% strain is about 50 KPa. In addition, the loading process shows three distinct regions, including the elastic region, the plateau region and the densification region due to the continuously decreasing pore volume, which is similar to the observation in literatures[17-19]. Even be compressed for 1000 cycles at strain of 70% (Fig. S4, Electronic Supplementary Information), the ADGA can still fully recover to its original volume and retain 65% of the first compressive stress. This suggests that the as-prepared graphene aerogel can be recycled as the compressive material. The original cyclic strain–stress curves for ten cycles at 70% strain are shown in Fig. 4b. The first compression cycle is different from the subsequent ones showing higher Young's modulus, maximum stress, large energy loss coefficient and work done by

compression (Fig. 4c). The hysteresis loop for the second cycle shrinks compared to the first one, but the max stress appearing at ε = 70% is only 8% lower than for the first one. Since the fifth cycle, the stress-strain curves almost remain unchanged. The first cycle yields a high energy loss coefficient of 0.85 and this coefficient remains constant at 0.68 since the fifth cycle. This property is very important for energy absorbing materials.[17-19] For the radial test, the maximum stress and Young's modulus are evidently less than that of axial loading at the same strain of 50% (Fig. 4d), which further demonstrated the oriented structure of ADGA. Moreover, the compressive stress and modulus can be controlled in a range by changing the GO concentration and increase along with the concentration (Fig. 4e).

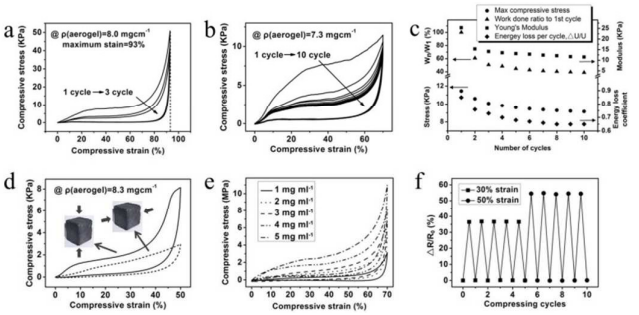

Fig. 4 The compression tests of ADGA. (a) The stress–strain curves of ADGA at the maximum strain of 93% for 3 cycles. (b) The stress–strain curves of ADGA at the strain of 70% for 10 cycles. (c) The corresponding Young's modulus, max compressive stress, work done and energy loss coefficient for different cycles derived from (c). (d) Different compressive stress–strain curves of a quadrate ADGA sample from two directions. (e) The stress–strain curves of ADGA as a function of concentration at the strain of 70%. (f) Electrical resistance change when repeatedly compressed up to 30% and 50% of strain for 10 cycles.

Benefiting from the superelasticity of ADGA, variable electrical resistance and recyclable absorbent for oil are the other applications for the compressive graphene aerogels. When the ADGA was connected in series by two metal plates with a battery and a lamp to form a simple circuit, it is obvious that the brightness of the lamp can be controlled by pressing the aerogel and the tighter the aerogel was squeezed, the brighter the lamp was (Fig. 3c). By measuring the electrical resistance of the unpressed aerogel and the aerogel pressed to 30% and 50% compressive strain several times, we know that the change in the electrical resistance is reproducible and the electrical resistance is only determined by the compressive strain (Fig. 4f). Thus, the ADGA may be applied in pressure sensing or stimulus-responsive graphene systems.[44, 45] The high porosity and hydrophobic nature of the aerogel mean that it is an excellent candidate for oil absorption. The organic solvent dyed with Oil Red floating on water and lying below the water can be absorbed completely by one ADGA (Fig. S5, Electronic Supplementary Information). Considering the strong connection and superelsticity of ADGA, we can recycle it by squeezing out the oil (Fig. S6, Electronic Supplementary Information). Of note, the height or the volume of the aerogel cannot recover until re-absorbing of the oil. Three cycles later, the red oil on the water were cleared. This way of squeezing out the oil is more efficient and environmental friendly than that of evaporating or burning it. Therefore, the ADGA can be used as recyclable absorbent for oil. This kind material makes human to process the oil leakage problem more efficiently and will benefit the environmental protection.

In summary, by combining the freeze-thaw technique and sol-gel method, i.e., carefully controlling the reduction degree of GO and selecting general freeze condition, we successfully prepared the ambient pressure dried graphene aerogel with superelasticity (rapidly recoverable from >90% compression). Thus prepared ADGAs exhibit oriented honeycomb-like structure with large pore size (ca.100~500 μm) and thick graphene walls (ca.200 nm). These special ADGAs have the best performance in superelasticity of graphene aerogels reported so far. Meanwhile, it is found that the ADGA also exhibits the variable electrical resistance and recyclable absorption capacity for oil based on its superelasticity, excellent conductivity and superhydrophobicity. Above all, the studies presented in this report would be a key progress for realizing the cost-effective and large-scale commercial production of high-performance graphene aerogels, which could be applied in many important fields such as energy dissipation, vibration damping, conductive sensor and recyclable absorbent for oil.

Acknowledgements

The authors acknowledge the financial support from Taishan Mountain Scholar Constructive Engineering Foundation (TS20081120 and tshw20110510) and Natural Science Fund for Distinguished Young Scholars of Shandong Province (JQ200905).

Notes and references

1 a) K. S. Novoselov, A. K. Geim, S. V. Morozov, D. Jiang, M. I. Katsnelson, I. V. Grigorieva, S. V. Dubonos, A. A. Firsov, *Nature*, 2005, **438**, 197. b) D. Li, R. B. Kaner, *Science*, 2008, **320**, 1170. c) A. K. Geim, *Science* 2009, **324**, 1530.

2 X. Cao, Y. Shi, W. Shi, G. Lu, X. Huang, Q. Yan, Q. Zhang, H. Zhang, *Small*, 2011, **7**, 3163-3168.

3 X. Cao, Z. Yin, H. Zhang, *Energ. Environ. Sci.*, 2014, **7**, 1850-1865..

4 S. Park, R. S. Ruoff, *Nature Nanotech.*, 2009, **4**, 217.

5 H. Bai, C. Li, G. Shi, *Advanced Materials*, 2011, **23**, 1089.

6 a) Y. Xu, G. Shi, *J. Mater. Chem.*, 2011, **21**, 3311. b) Z. Yin, J. Zhu, Q. He, X. Cao, C. Tan, H. Chen, Q. Yan, H. Zhang, *Adv. Energy Mater.*, 2014, **4**, 1300574. c) X. Huang, Z. Zeng, Z. Fan, J. Liu, H. Zhang, *Adv. Mater.*, 2012, **24**, 5979-6604.

7 a) H. Bai, C. Li, X. L. Wang, G. Shi, *J. Phys. Chem. C*, 2011, **115**, 5545. b) X. Huang, X. Qi, F. Boey, H. Zhang, *Chem. Soc. Rev.*, 2012, **41**, 666-686. c) X. Huang, Z. Yin, S. Wu, X. Qi, Q. He, Q. Zhang, Q. Yan, F. Boey, H. Zhang, *Small*, 2011, **7**, 1876-1902.

8 H. Jiang, P. S. Lee, C. Li, *Energ. Environ. Sci.*, 2013, **6**, 41.

9 H. X. Kong, Curr. Opin. Solid State Mater. Sci., 2013, **17**, 31.

10 Y. Zhao, C. Hu, Y. Hu, H. Cheng, G. Shi, L. Qu, *Angewandte Chemie*, 2012, **124**, 11533.

11 V. Chabot, D. Higgins, A. P. Yu, X. C. Xiao, Z. W. Chen, J. J. Zhang, *Energy Environ. Sci.*, 2014, **7**, 1564.
12 C. Li, G. Shi, *Nanoscale*, 2012, **4**, 5549.
13 S. Nardecchia, D. Carriazo, M. L. Ferrer, M. C. Gutierrez, F. del Monte, *Chem. Soc. Rev.*, 2013, **42**, 794.
14 M. A. Worsley, P. J. Pauzauskie, T. Y. Olson, J. Biener, J. H. Satcher, T. F. Baumann, *J. Am. Chem. Soc.*, 2010, **132**, 14067.
15 X. Zhang, Z. Sui, B. Xu, S. Yue, Y. Luo, W. Zhan, B. Liu, *J. Mater. Chem.*, 2011, **21**, 6494.
16 W. Chen, L. Yan, *Nanoscale*, 2011, **3**, 3132.
17 L. Qiu, J. Liu, S. Chang, Y. Wu, D. Li, *Nat. Commun.*, 2012, **3**, 1241.
18 H. Hu, Z. Zhao, W. Wan , Y. Gogotsi, J. Qiu, *Advanced materials*, 2013, **25**, 2219.
19 J. Li, J. Li, H. Meng, S. Xie, B. Zhang, L. Li, H. Ma, J. Zhang, M. Yu, *J. Mater. Chem. A*, 2014, **2**, 2934.
20 Y. Li, J. Chen, L. Huang, C. Li, J. Hong, G. Shi, *Advanced Materials*, 2014, **26**, 4789.
21 S. Barg, F. M. Perez, N. Ni, P. V. Pereira, R. C. Maher, E. Garcia-Tun˜on, S. Eslava, S. Agnoli, C. Mattevi, E. Saiz, *Nat. Commun.*, 2014, **5**.
22 R. Zhang, Y. Cao, P. Li, X. Zang, P. Sun, K. Wang, M. Zhong, J. Wei, D. Wu, F. Kang, H. Zhu, *Nano Research*, 2014, **7**, 1477.
23 H. Sun, Z. Xu, C. Gao, *Advanced Materials*, 2013, **25**, 2554.
24 C. Lee, X. Wei, J. W. Kysar, J. Hone, *Science*, 2008, **321**, 385 .
25 M. Huang, T. A. Pascal, H. Kim, W. A. Goddard, J. R. Greer, *Nano Lett.*, 2011, **11**, 1241.
26 S. Yun, H. Luo, Y. Gao, *RSC Advances*, 2014, **4**, 4535.
27 K. Guo, Z. Hu, H. Song, X. Du, L. Zhong, X. Chen, *RSC Advances*, 2015, **5**, 5197.
28 M. Liu, L. Gan, Y. Pang, Z. Xu, Z. Hao, L. Chen, *Colloids and Surfaces A: Physicochemical and Engineering Aspects*, 2008, **317**, 490.
29 F. Shi, L. Wang, J. Liu, *Materials letters*, 2006, **60**, 3718.
30 D. Wu, R. Fu, S. Zhang, M. S. Dresselhaus, G. Dresselhaus, *Carbon*, 2004, **42**, 2033.
31 S. D. Bhagat, C. S. Oh, Y. H. Kim, Y. S. Ahn, J. G. Yeo, *Microporous and mesoporous Materials*, 2007, **100**, 350.
32 J. Zarzycki, M. Prassas, J. Phalippou, *J. Mater. Sci.*, 1982, **17**, 3371.
33 S. Deville, E. Saiz, R. K. Nalla, A. P. Tomsia, *Science*, 2006, **311**, 515.
34 H. Zhang, I. Hussain, M. Brust, M. F. Butler, S. P. Rannard, A. I. Cooper, *Nat. mater.*, 2005, **4**, 787.
35 K. M. Pawelec, A. Husmann, S. M. Best, R. E. Cameron, *Applied Physics Reviews*, 2014, **1**, 021301.
36 B. Wicklein, A. Kocjan, G. Salazar-Alvarez, F. Carosio, G. Camino, M. Antonietti, L. Bergström, *Nat. Nanotechnol.*, 2014.
37 T. A. Schaedler, A. J. Jacobsen, A. Torrents, A. E. Sorensen, J. Lian, J. R. Greer, L. Valdevit, W. B. Carter, *Science*, 2011, **334**, 962.
38 T. M. Tillotson, L. W. Hrubesh, *J. Non-Cryst. Solids*, 1992, **145**, 44.
39 B. C. Tappan, M. H. Huynh, M. A. Hiskey, D. E. Chavez, E. P. Luther, J. T. Mang, S. F. Son, *J. Am. Chem. Soc.*, 2006, **128**, 6589.
40 D. A. Dikin, S. Stankovich, E. J. Zimney, R. D. Piner, G. H. Dommett, G. Evmenenko, S. T. Nguyen, R. S. Ruoff, *Nature*, 2007, **448**, 457.
41 H. Chen, M. B. Müller, K. J. Gilmore, G. G. Wallace, D. Li, *Advanced Materials*, 2008, **20**, 3557.
42 J. Zhang, H. Yang, G. Shen, P. Cheng, J. Zhang, S. Guo, *Chem. Commun.*, 2010, **46**, 1112.
43 J. Li, B. Zhang, L. Li, H. Ma, M. Yu, J. Li, *Radiat. Phys. Chem.*, 2014, **94**, 80.
44 Y. Zhao, L. Song, Z. Zhang, L. Qu, *Energy Environ. Sci.* 2013, **6**, 3520.
45 Y. Deng, J. Zhang, Y. Li, J. Hu, D. Yang, X. Huang, *J. Polym. Sci., Part A-1: Polym. Chem.* 2012, **50**, 4451.